Engineered porosity-induced burn rate enhancement in dense Al/CuO nanothermites

Tao Wu, Baptiste Julien, Haiyang Wang, Sylvain Pelloquin, Alain Estève, Michael Zachariah, Carole Rossi

Engineered porosity-induced burn rate enhancement in dense Al/CuO nanothermites

*Tao Wu, Baptiste Julien, Haiyang Wang, Sylvain Pelloquin, Alain Esteve, Michael R. Zachariah, Carole Rossi**

Author information

Corresponding Author

Carole Rossi – LAAS-CNRS, University of Toulouse, 31077 Toulouse, France ; orcid.org/0000-0003-3864-7574; E-mail: rossi@laas.fr

Authors

Tao Wu – LAAS-CNRS, University of Toulouse, 31077 Toulouse, France; orcid/org/0000-0003-3704-275X

Baptiste Julien - LAAS-CNRS, University of Toulouse, 31077 Toulouse, France; orcid.org/0000-0002-4297-3455

Haiyang Wang – University of California, Riverside, Riverside, California 92521, United States; orcid.org/0000-0001-5200-3965

Sylvain Pelloquin – LAAS-CNRS, University of Toulouse, 31077 Toulouse, France; orcid.org/0000-0001-5963-2852

Alain Esteve – LAAS-CNRS, University of Toulouse, 31077 Toulouse, France

Michael R. Zachariah – University of California, Riverside, Riverside, California 92521, United States; orcid.org/0000-0002-4115-3324;

Abstract

This work investigates the combustion of porous Al/CuO thermites, i.e. nanolaminates fabricated with various densities of micron sized air-filled pores in the range of 0 - 20 vol%. High-speed videography and pyrometry of the high-temperature propagating flame were used to analyze the effect of porosity on propagation velocity. Incorporating micron sized pores in Al/CuO nanolaminates results in a faster burn rate (burn rate enhancement of 18% for pores loading of 20 vol%) while the flame temperature remains the same. Microscopic observations of the flame front in porous nanolaminates show hot-spots around each pore in the upstream of the flame but no advection. Conduction remains the dominant heat transfer mechanism in dense thermite configuration (80 % TMD) and the causes of burn rate enhancement when pores are

embedded into the nanolaminate are found to be the convection of the trapped air inside the pores upon heating together with a possible modification of the reaction chemistry leading to a lowering of the ignition threshold of thermite around each micron sized pores. Indeed, this hot gaseous O_2 species trapped into the pores diffuse and react with solid Al on the inner wall of the pores to form Al_2O_3. This This gas phase mediated reaction mechanism in the pores occurs at a lower temperature than the diffusion-based mechanism of the aluminum cations and oxide anions across the alumina shell as in fully dense Al/CuO nanolaminates. The critical size of the pores beyond which their beneficial effect disappears is difficult to estimate, but, this study showed that 100 × 100 μm² pores has almost no effect on the combustion with an average burn rate increase of only ~4% compare to fully dense nanolaminate part.

KEYWORDS: nanothermites, porous nanolaminate, Al/CuO, combustion, flame propagation, heat transfer, advection, convection

1. Introduction

Since the 1990s, the progress in nanomanufacturing [1] has led to a new class of solid energetic materials commonly referred to as nanoscale composite energetic materials, or simply nanoenergetics. These materials include nanothermites composed of nanosized metals (Al, Mg, Ti, and B) and metal oxides (CuO, Fe_2O_3, Bi_2O_3, and MoO_3…), which both participate in a highly exothermic and self-propagating redox reaction [2, 3]. Much research in nanothermites have focused on the Al/CuO systems due to their high energy density [4, 5], and because they allow fabricating thermite systems with varying shapes/geometries, i.e. multilayered [6, 7], core/shell [8, 9] , 3D assembled particles [10, 11] , and 3D porous nanostructures [12]. It has been observed that the formulation and deposition method greatly affect the energy transfer mechanisms and combustion behavior, which depend on several factors, such as reactant intimacy, material confinement or gas generation. This performance tunability in addition to

the high energy density make nanothermites promising for joining or welding [13] tunable generators of biocidal-agents [14, 15], actuation in initiators/detonators [16, 17] and in single-use miniaturized microelectromechanical systems [18-21] such as microthrusters [22, 23].

Despite the over 3 decades of experimental and theoretical research in the field of nanothermites, relatively little is known of the energy transfer mechanisms governing the self-propagation of the reaction front. They depend on several factors such as the gas products generated, the heat transfer mechanisms, i.e., conduction (transport of heat within the material itself), convection (transfer of heat by the physical movement of hot masses of gas) or advection (physical movement of solid or molten aggregates); the activation energies of the reactive components and material confinement. In confined environments and in low-density thermite configurations (powder with compaction < 50% of the theoretical maximum density, TMD), convection of hot gases and ballistic advection of condensed phase aggregates [24, 25] are the dominant heat transfer mechanisms during flame propagation, whereas pure conduction (or normal deflagration) prevails at higher densities. This was supported by experimental findings showing that loosely packed nanothermite powders propagate from ∼100 m/s to ∼km/s [26-29] against ∼cm/s to ∼m/s for fully dense laminated nanothermites [30]. No data is yet available on heat transfer mechanisms governing the self-propagation of dense thermite configurations i.e. powder with compaction > 75% TMD, due to technical impossibility to obtain nanopowders at that compaction rate.

The objective of this paper is both to examine the effect of porosity on the combustion in high-density thermite configurations (> 75% TMD), and to elucidate which of the heat transfer mechanisms among conduction, convection or advection, is dominant in such configurations. For that purpose, controlled porosity, i.e. a controlled quantity of air-filled pores, 10 × 10 μm² in size, are embedded into fully dense Al/CuO nanolaminates through a simple photolithography approach. The self-propagation of the reaction front in such prepared

materials containing various fractions of pores in the range of 0 - 20 vol%, is observed at the macro and microscale and compared with fully dense nanolaminates. It is found that a small fraction (~20 vol%) of 10 × 10 µm² pores within the nanolaminate accelerates the burn rate by ~18%. *In operando* microscopic observations of the confined burning flame front shows the formation of hotter zones (hot-spots) in and around the pores, whereas no advection is observed through them. Therefore, the formation of hot-spots in the upfront is supposed to result from two mechanisms: the convection of the heated air trapped inside the pores enhancing the heat transfer to unreacted nearby material; and the interaction of diffused free-molecular oxygen species from the trapped air with solid Al on the inner wall of the pores to form Al_2O_3. This gas-phase reactional pathway is kinetically more favorable than the purely condensed phase reactional mechanism occurring at the Al/CuO interface in fully-dense thermite systems. [31] This study also outlines that the beneficial effect of air-filled pores is greatly reduced when increasing pores size up to 100 × 100 µm² as the mass of trapped air in the pore becomes too large to be heated at a sufficient temperature to establish convection.

2. Materials and methods

2.1. Porous nanolaminate samples fabrication

Lines of nanolaminates with dimensions of ~30 mm (length) × 4 mm (width) were sputter-deposited onto a ~31.75 mm (length) × 17.75 mm (width) × 500 µm (thick) glass slide (**Figure S1**). Titanium filaments were patterned at both nanolaminate ends, underneath the nanolaminate line, to resistively heat the multilayer to ignition (**Figure S1**). The nanolaminates used in this work consist of 13 Al/CuO bilayers deposited using a direct current (DC) magnetron-sputtering system from TFE (Thin Film Equipment, Italy). Al and CuO were sputtered from Al and Cu targets (8 by 3-inch square sides and ¼ inches thick) using a base pressure of 5.10^{-7} mbar. O_2 and Ar gas flow rates of 16 and 32 cm^3/min were used for CuO deposition with a partial pressure

of 10^{-2} mbar. The Ar partial pressure during Al deposition was maintained at 5.10^{-3} mbar. The sample was cooled at ambient temperature for 600 s at the end of the deposition process. The percentage of porosity added into the fully dense Al/CuO nanolaminate was controlled by varying the volume loadings of 10 × 10 µm² cavities into the material, as depicted in **Figure 1a-c**. As the first step, a negative photoresist (NLOF2070, MicroChemicals, 20 µm) was spin-coated onto the glass wafer to obtain a 10 µm thick NLOF layer. This photoresist layer was soft baked at 110 °C for 2.5 min and cooled down to room temperature. The photoresist layer was then patterned by exposing it under UV light (A6 Gen4 Suss Microtec, 360 mJ/cm²) through a contact mask defining the porosity patterns. After a post-bake at 125 °C for 3 min, the pattern was then transferred to the photoresist layer by developing the exposed photoresist using a MF-CD-26 developer for 130 s, followed by rinsing in deionized water, and dried under N_2. Then, the Al/CuO nanolaminate was sputter-deposited. To remove the photoresist pillars and reveal the pore, the sample was put into an acetone bath for 3 h followed by another 10 min of sonication. After this step, we end up with Al/CuO nanolaminates embedding open cavities as shown in **Figure 1c**. Next steps consist in the hermetic sealing of the air into the cavities to produce close pores. A 5 µm thick dry film (DF 1005, SU8 epoxy-based photoresist) was laminated on Al/CuO nanolaminate by a laminator (Shipley 3024) with a rolling speed of 1 $m.s^{-1}$, a rolling pressure of 2.5 bars, and a temperature of 90 °C. Then the DF coated nanolaminate was exposed at UV light and followed by a development to remove the extra DF part on the chip in order to expose the ignition contacts. Then the DF-sealed Al/CuO nanolaminate was covered with a layer of resin (Pack resin MA2+, PRESI, France) (**Figure 1d**). SEM cross-sections of the sealed Al/CuO nanolaminate with 20% porosity are shown in **Figure 1e-f** showing the cavities sealed by the DF and resin covers. The dimensions of the pores are measured to be 9 × 9 µm² instead of 10 × 10 µm². Four porosity configurations are considered in this study: 3, 9, 14 and 20% loading (**Table S1)**. For comparison purposes, required for

results analysis, an additional set of samples was prepared in which the dimension of the pores was increased to 100 × 100 µm² keeping the fraction at 20%. If not specified, the Al/CuO bilayer thickness is set at 300 nm with an Al to CuO equivalence ratio of 2:1 (fuel-rich configuration), i.e. Al and CuO thicknesses of 150 nm, respectively.

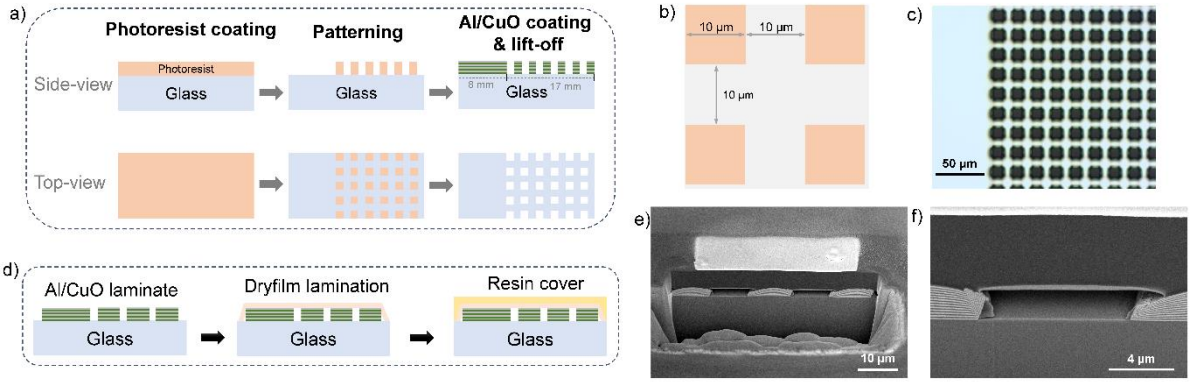

Figure 1. *(a) Schematic of the process developed to obtain air cavities (pores) within Al/CuO sputter-deposited nanolaminates; (b) Zoom of the photolithography mask pattern used to obtain 20% porosity; (c) an optical top view image of a Al/CuO nanolaminate with 20% porosity; (d) schematic of the encapsulation process to obtain the porous laminates, i.e. sealed with a dry epoxy film and covered with a resin layer; (e-f) SEM cross-section images of a sealed Al/CuO nanolaminate with 20% porosity.*

It has to be noted that, for all samples, the first third of the nanolaminate length, 10 mm long, does not contain pores and allows measuring a reference burn rate (i.e. a fully dense Al/CuO nanolaminate average burn rate). The other two-thirds (20 mm) of the nanolaminate length contains the pores and thus constitutes the porous part.

2.2. Characterization

Material observations. The structures and compositions of the Al/CuO laminates as well as the reaction products were characterized by scanning electron microscopy (SEM, FEI Helios 600i Nanolab), coupled with energy-dispersive X-ray spectroscopy (EDX). The post-product was characterized by SEM (Hitachi, S-4800) and EDX. The particles sizes were measured by

ImageJ over 50 particles on several SEM images. The working distance is 8 mm, with an in-lens SE/BSE detector (TLD) and an accelerating voltage of 5 kV.

Macro-scale combustion tests. To evaluate the flame propagation speed of the Al/CuO nanolaminates; referred to as the average burn rate, the prepared samples were imaged with a high-speed camera (25 cm) (Phantom VEO710L-18GB-M, USA) at 94,000 frames/s. Around six burn rate experiments were carried out per sample configuration and all experiments were performed in a constant-pressure air atmosphere. An average burn rate was then calculated by tracking the distance travelled by the reaction front as a function of time by Phantom Camera Control software (6 positions in the flame front were used for each burn rate experiment and then an average value was obtained). And, for each sample configuration, two average burn rates were calculated: v_1 and v_2 in the fully dense part and in porous part of the nanolaminate, respectively. Then, the flame propagation speed percentage deviation ($\Delta \boldsymbol{v}$) is deduced using Eq. 1.

$$\Delta \boldsymbol{v}\ (\%) = \frac{\boldsymbol{v_2 - v_1}}{\boldsymbol{v_1}} \times \mathbf{100} \qquad \text{Eq. 1}$$

High-speed microscopy/pyrometry. The details of the flame front propagation of the Al/CuO nanolaminates were observed *in-operando* using a high-speed microscopic imaging system. Detailed information can be found in previous studies[32-34]. For short, a high-speed camera (Vision Research Phantom VEO710L, USA) coupled to a long-distance microscope (Infinity Photo-Optical Model K2 DistaMax, USA) that provides a pixel/distance ratio of 2.2 µm/pixel to observe the flame front propagation (77000 frames/s). The high-speed microscope apparatus has also been calibrated with a blackbody source for color pyrometry to estimate the temperature of the reaction. The detailed information about the color ratio pyrometry could be found in previous study [42]. The temperature uncertainty is estimated to be 200−300 K.

3. Results and discussion

3.1. Enhanced average burn rate of porous Al/CuO laminates

The flame propagation of Al/CuO nanolaminates with various pores fraction (3, 9, 14 and 20%) was investigated by high-speed videography. Steady state propagation is achieved within ~3 mm of the nanolaminate length. **Figure 2a-d** shows the typical time-resolved snapshots of their propagation in both the fully dense reference and the porous fraction; noted that the burn rates were not determined from those frames (see **Section 2.2** for details). Importantly, for all four laminates regardless of their pores content, the porous material burns slightly faster than the fully dense reference one. The samples with 20% porosity burn at an average rate of ~23.9 ± 2.0 $m.s^{-1}$, which corresponds to a ~18% increase compare to the reference (~20.2 ± 1.8 $m.s^{-1}$). However, the flame temperature is measured at ~2410 °C in the porous part, i.e. similar to that of the fully dense Al/CuO case (~2300 °C). The propagation speed variation versus the pores content is plotted in **Figure 2e**: an increase of pores content from 3 to 9% causes the burn rate change to rapidly rise from ~3% to ~17%, before plateauing at ~20% pore content. Importantly, the snapshots show that the reaction front, approximately 200 µm thick for all samples, becomes corrugated when entering into the porous side of the sample: the front generally adopts a "L" or "V" shape, with front edges pointing to the upfront. The corrugation, which is defined by the ratio of the total geometrical length of the flame to the width of the sample in the direction perpendicular to propagation, increases with pores content from 1.2 to 2. Corrugation is meant to characterize the degree of roughness of the flame front. Similarly to what was reported in [34], we observe that corrugation goes with an increase of the average burn rate. Considering that flame propagation behavior, i.e. its corrugation, is dependent on how fast energy is generated (kinetics of the reaction) and how fast that released energy can be transferred to unreacted area (heat transfer mode), the corrugation of the flame front obtained on porous nanolaminates is the consequence of either a lowering of the ignition threshold by the presence of free molecular oxygen in the pores, or, an enhancement of heat transfer through the pores by advection and/or convection; indeed, we can imagine that the heat

would transferred through the air-filled cavities by the movement of condensed phase aggregates travelling through the cavities and/or the air trapped inside the pores, thus preheating or initiating the upfront (side and opposite side walls of microcavities) faster than the thermal wave by conduction. To probe if advection/convection occurs during combustion in porous nanolaminates, we now turn our attention to a microscopic view of the flame front with a resolution of ~2.2 μm/pixel.

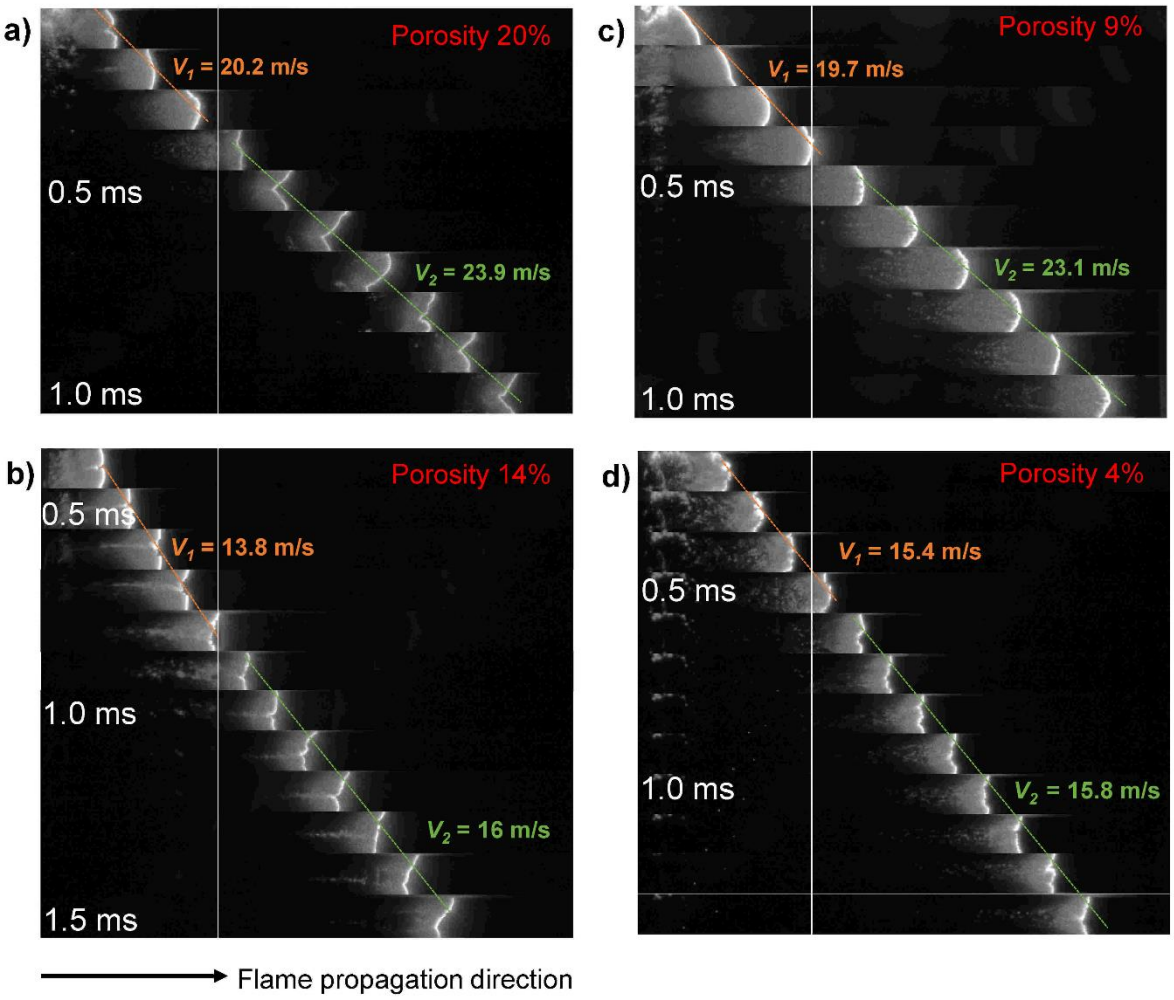

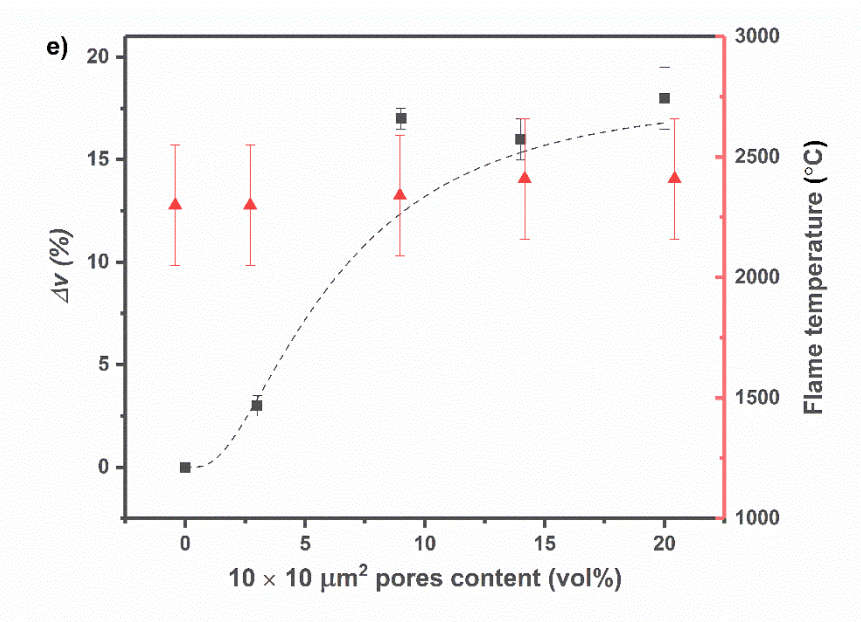

Figure 2. *High-speed images of the propagating flame front for Al/CuO nanolaminates with (a) 20%, (b) 14%, (c) 9%, and (d) 4% porosity, respectively; (e) corresponding percentage of*

propagation speed changes and flame temperatures. The Al to CuO equivalent ratio is 2:1. White vertical lines on the video images delimits the fully dense (left-side) to porous part (right side).

3.2. Microscopic imaging of the flame front with pyrometry

The propagating flame front in the porous region was observed around the air-filled cavities using a much higher spatial (~2.2 µm/ pixel) and temporal (µs) resolution coupled with pyrometry. **Figure 3a-b** snapshots obtained on samples with 20% porosity confirm that the front is corrugated when entering into the porous region and the temperature is confirmed at 2410 °C. The shape and image of the confined flame front in **Figure 3b** show that the whole pores are hotter (+~500°C) than the surrounding fully dense Al/CuO, which implies the air trapped inside the pores in the flame front are heated and convection of hot air could play a role in propagation. However, high-speed microscopy images do not allow distinguishing advection of particles of burning matter flying away through the cavities. Because the size of the pores is near the limit of our optical resolution, and the propagation is so fast that we could only obtain 1 to 3 frames, which is insufficient to accurately capture any advection events. We therefore produce nanolaminates with pores'size 100× larger, i.e. 100 × 100 µm² keeping the same volume fraction (20%), and probe the flame front propagating around the air-filled pores.

Images in **Figure 3c-d** show that some advection does appear in only a few large pores (~20%). **Figure 3e-f** further indicate that the flame preferably propagates through the dense thermite without advection. But, interestingly the pores are not hotter than the Al/CuO bulk as observed in samples with 10 × 10 µm² pores (**Figure 3b)** and the average burn rate of porous nanolaminates with embedded 100 × 100 µm² pores does not increase much compare with the reference material (only 4% increment). Results thus suggest that the influence of advection on the flame propagation in this material is negligible.

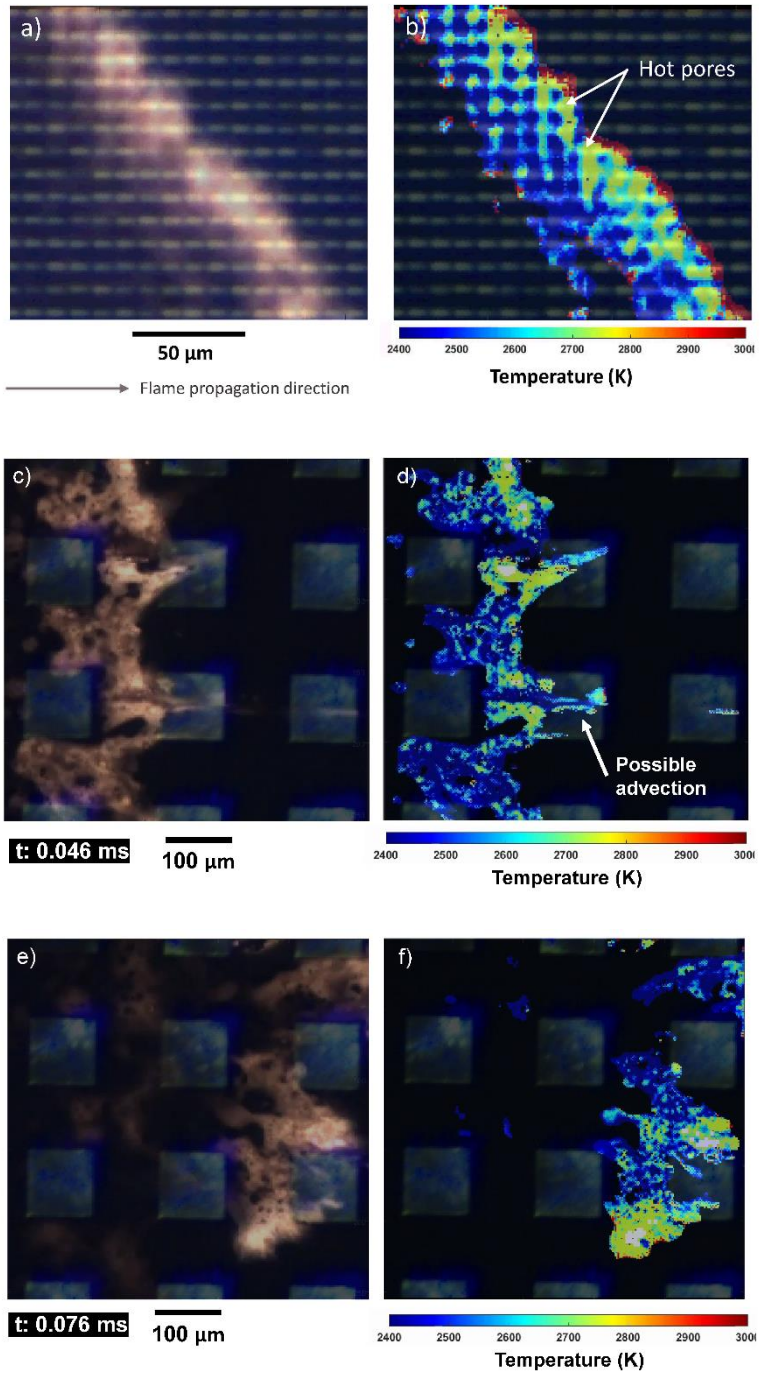

Figure 3. *Microscopic imaging of the propagating flame front for Al/CuO nanolaminates with (a and b) 20 vol% of 10 × 10 µm² pores, (c-f) 20 vol% of 100 × 100 µm² pores; zoom in two 100 × 100 µm² air-filled pores where (c and d) some advection is visible, (e and f) without advection. The Al to CuO equivalent ratio is 2:1.*

Rather, in the absence of advection, hot-zones around 10 × 10 µm² pores seen on microscopic observations of the flame front may indicate faster burn rate would result from 2

joint effects: 1) the establishment of convection of the trapped air (and possibly gaseous copper since its boiling point is in the order of the flame temperature) inside the pores, thus improving the heat and mass transfer to unreacted nearby laminate; 2) a modification of the redox reaction pathway lowering the ignition threshold at the pore edges. Note that the "hot" air trapped inside the pores is a strong oxidizer and thus will react with exposed Al following a gas-phase or gas-surface exothermal reaction mechanism. In literature [31] investigating arrested reactive milled Al/CuO nanocomposites containing nanovoids, the authors showed that incorporation of micron sized pores into dense Al/CuO thermites lowers the ignition threshold compared to fully dense composite. The authors conjectured that gaseous O_2 species diffuse through the pores and react readily upon adsorbing to exposed Al or Al_2O_3. Importantly, this work highlighted that the reaction scenario of free molecular O_2 reaction with exposed solid Al or Al_2O_3 leading to the formation of Al_2O_3 and Cu is more thermodynamically favored compared to the purely condensed phase mechanism dominating the reaction at the interfaces of Al and CuO [35] as in a fully dense Al/CuO laminates. [4, 6, 36, 37]

Observations differ in porous laminates embedding 100 × 100 µm² pores (**Figure 3e-f):** convection failed to establish in the pores as they remain at the same temperature as bulk Al/CuO. The energy delivered by the burning reaction front is insufficient to heat up the trapped air mass (increased by × 10 compared to small pores) over 650 K. In addition, the large pores feature larger inert surface areas (top resin and bottom glass covers), so that the heat loss for each individual pore is more significant than the smaller pores. But, the burn rate of porous laminates with large pores (20 vol%) is enhanced by 4% compared to bulk Al/CuO: this increment may be the contribution of the lowering of the ignition threshold at the pore edges due to the presence of gaseous oxidizer.

3.3. Post-combustion products analysis

To further analyze the relevance of this conjecture the post-combustion products collected from fully dense and porous (containing 20 vol% of 10 ×10 μm² pores) 1:1 nanolaminates (Al thickness 100 nm and CuO thickness 200 nm) were retrieved by a carbon tape and then characterized using scanning electron microscopy. **Figure 4** shows the different particle morphologies from the collected post-combustion residues. In all SEM images, the brighter spherical particles are identified as Cu and the grey Al_2O_3, based on the corresponding EDX analysis shown in **Figure 5**. Interestingly, for all samples, post-combustion products are composed of two different populations: large micron sized particles (size given in **Table 1**) and clusters of aggregated nanoparticles being 100 – 400 nm in size. EDX analysis of the nanoparticles identify them as individual Cu and Al_2O_3 nanoparticles **(Figure 5i-l)**. These nanoparticles collected in both laminates are condensed reaction products (Cu and Al_2O_3), which were able to be accessed because the whole combustion event happened within a sealed space, whereas laminates burning in an open atmosphere [30] produce only large particles of Al_2O_3, Cu or Al/Cu alloys.

Two major differences can be highlighted on large residues collected from porous and fully dense laminates. First of all, Cu and Al_2O_3 products after combustion of the fully dense laminate feature a snowman-like shape (usually Cu on top and Al_2O_3 at bottom). By contrast, Cu and Al_2O_3 products after combustion of porous laminate are mostly separated particles with some Cu particles deposited on the surface of Al_2O_3. Secondly, both Cu and Al_2O_3 products collected from porous laminates feature larger sizes than the ones collected from the fully dense samples, as summarized in **Table 1.**

Although, the analysis of residues size and composition does not give a direct evidence of the convection of trapped air inside the pores and/or the lowering of the ignition threshold, the observations are aligned with the previous comments regarding to the overall reaction scenarios. In the fully dense nanolaminate, a condensed phase reaction at the Al/CuO interface

seems to dominate the reaction because the produced Cu particles are always attached to Al_2O_3 particles. Noticeably, there are much fewer Cu/Al_2O_3 agglomerates in the combustion products of porous laminates. Obviously introducing 10 × 10 μm^2 pores within the laminate reduces reactants and products agglomeration which in turn enhances the burn rate of nanothermites as already observed in [32, 38]. The size enlargement observed in porous zones is also consistent with the following two facts: 1) there is more space available for the products to eject to in the porous zones; 2) the trapped air inside the pores can potentially facilitate the oxidation of Al and improve the overall burn rate.

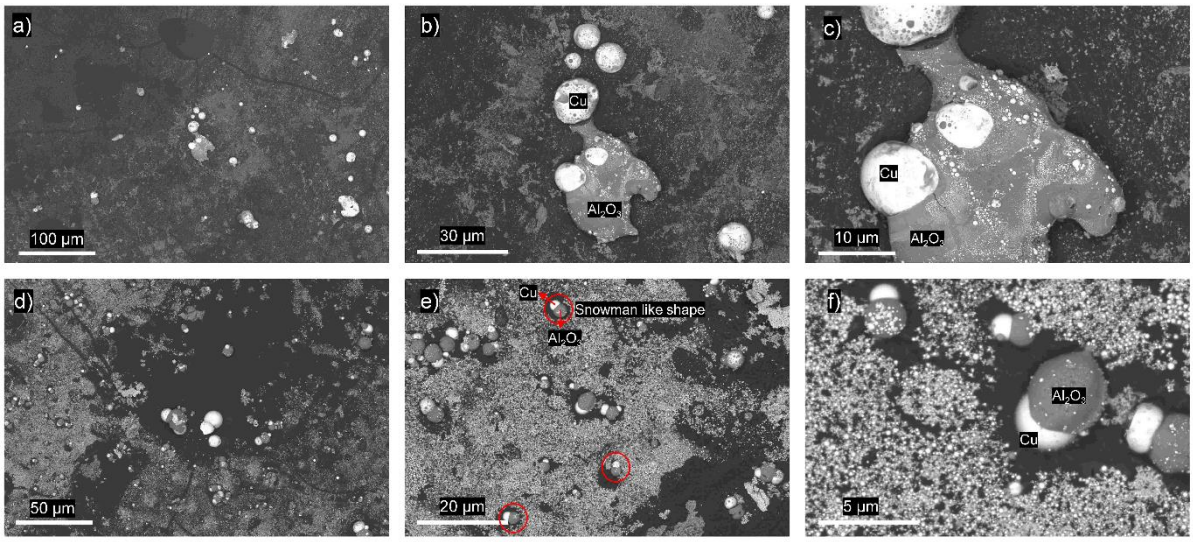

Figure 4. *SEM images of combustion residues collected after the combustion of (a-c) 1:1 Al/CuO nanolaminate with 20% air-filled porosity, (d-f) fully dense 1:1 nanolaminate.*

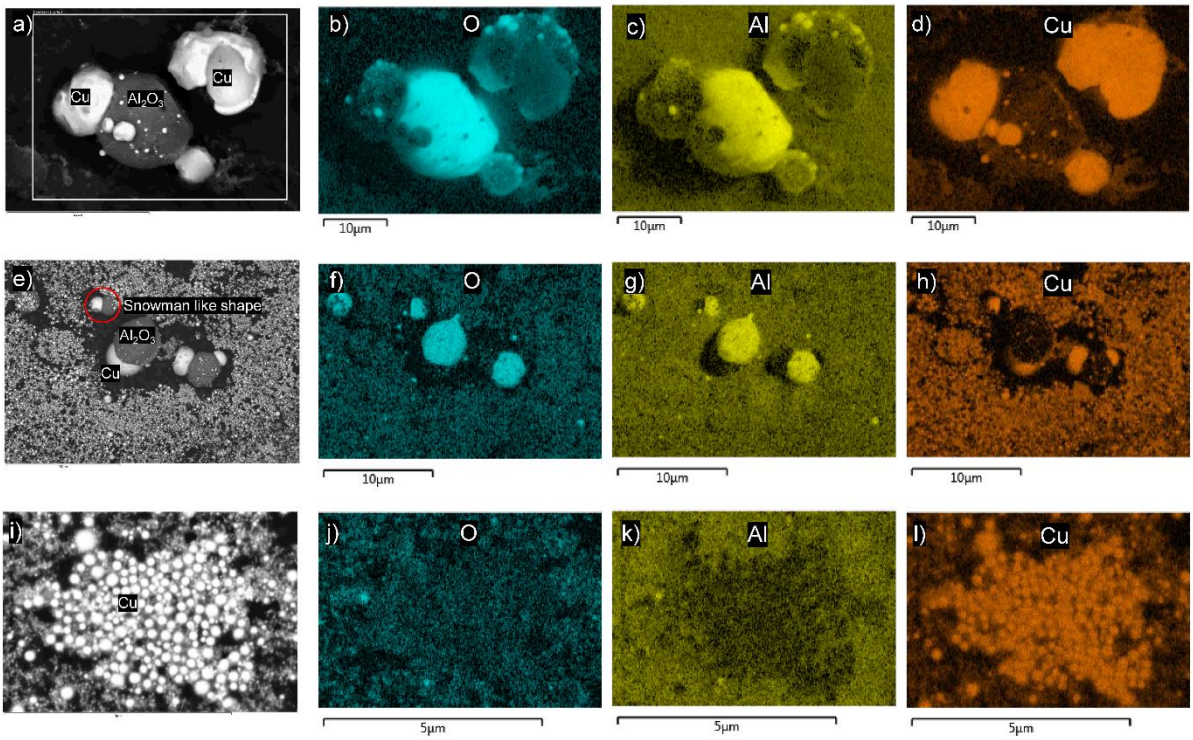

Figure 5*. EDX mapping results of post-combustion products collected from (a-d) 1:1 Al/CuO nanolaminate with 20% air-filled porosity, (e-h) fully dense 1:1 nanolaminate, (i-l) nanoparticles from fully dense nanolaminate.*

Table 1. Summarizing size distributions of post-combustion products (large particles only).

Post-combustion products	**Size (µm)**	
	Cu	**Al_2O_3**
Porous nanolaminate	8.5 ± 5.1	16.2 ± 8.5
Fully dense nanolaminate	1.6 ± 0.8	2.5 ± 1.0

3.4. Flame propagation modeling in porous nanolaminates

As a final step of this study, a two-dimensional (2D) and time-dependent heat diffusion model (Eq. 2) was built to explore the effect of porosity on the burn rate considering the two possible scenarios: molten-product advection though pores, and formation of hot-zones upstream of the flame due to a local enhancement of the reactivity i.e. earlier redox reaction ignition at pore edges. The flame propagation in dense nanolaminate being a purely conductive process, a purely conductive model is employed as in [39]. For simplicity, the exothermic Al+CuO

reaction is simulated by a source term, and the model assumes that no exothermic self-heating reaction occurs prior to the ignition point, assumed to occur at a certain temperature, as discussed below. Noted that the reaction kinetic, which corresponds to the time the material takes to react after being heated to its ignition temperature is not considered. Then, the system is described by the time-dependent diffusion equation:

$$\frac{\partial T}{\partial t} - \alpha(\Delta T) = \frac{S}{\rho c} \qquad \text{Eq. 2}$$

where ρ, c and α are the density, specific heat and thermal diffusivity of the Al/CuO nanolaminates. For each node (i,j), the thermal properties are calculated as $\lambda_{i,j}$, $\rho_{i,j}$ and $c_{i,j}$. Then, for each time step n, the node temperature is calculated by a finite element method. As initial condition, the nanolaminate is ignited at the left ($i = 0$), i.e. a temperature of 2843 K is set at the left boundary, corresponding to the adiabatic temperature of the Al/CuO reaction and copper vaporization point. In other words, $T^0_{0,j}$ = 2843 K, while in the rest of the laminate, $T^0_{i\neq 0,j}$ is initially set at the ambient temperature, 298 K. Since the goal of this study is not to quantify burn rates but rather support qualitatively experimental tendencies, no heat loss is considered. The heat source term, $S_{i,j}$ is also arbitrarily set at 2×10^5 W.m^{-3} in order to fit the experimental burn rate measured on the fully dense Al/CuO nanolaminate reference region: ~20 m.s^{-1}. $S_{i,j}$ is null inside the pores. The average thermo-physical properties and condition parameters used in the calculations are given in **Table S2** and **Table S3**. Simulation outputs is the 2D temperature field/map for each conditions (only thermal conduction, advection added in pores, lower ignition threshold around pores) and at different simulation times, as shown in **Figure 6a**. The average burn rate is then determined as the distance between the points where the temperature reaches the flame temperature (2843 K) and the minimum temperature (ambient). The predicted average burn rate is plotted in **Figure 6b** for nanolaminate with porosity varying from 4 to 20% considering the two distinct scenarios:

(1) the ignition threshold is lowered around each pore to simulate a possible reduction of the activation energy of oxygen diffusion due to the convection of gaseous O_2 in the pores. In other words, the ignition temperature is set at 650 K at the vicinity of the pores whereas it is set at 1050 K in the bulk, according to a previous work [40] (**Figure 6c, green dashed line).** In this paper, vicinity is defined by a ring around the hole; considering a 10 µm² pore, a ring of 1 µm wide is set around the hole, which is the vicinity of this pore.

(2) heat transfer is enhanced through the cavities by advection of molten products. Thus, a spontaneous transmission of the heat from the wall in contact with the flame front to the other walls (two sides walls plus the opposite one) is implemented (**Figure 6c, black dashed line)**. Note that this is a simplification of the real advection processes as we consider the time of flight of potential aggregates throughout the cavities equal to zero, but it aims at evaluating the order magnitude of the flame speed change as a function of pores fraction.

Simulation results show that advection mechanism has a much greater effect on burn rate enhancement than chemistry: with an increase of air-filled pores content from 4 to 20%, the propagation speed rapidly increases from ~10% to ~40% when advection is added, against less than 10% if we consider that the presence of free molecular oxygens inside the pores reacts with surrounding Al at lower temperature than in a purely condensed phase reactional mechanism i.e. when occurring at the fully dense Al/CuO interface. Increasing the size of pores to 100 × 100 µm² leads to an increase of burn rate of 70% against ~1.5% (not plotted in graph of **Figure 6b**) considering an earlier ignition threshold at pore edges. This also corroborates qualitatively the experimental findings and highlights the fact that convection plays a role in burn rate enhancement.

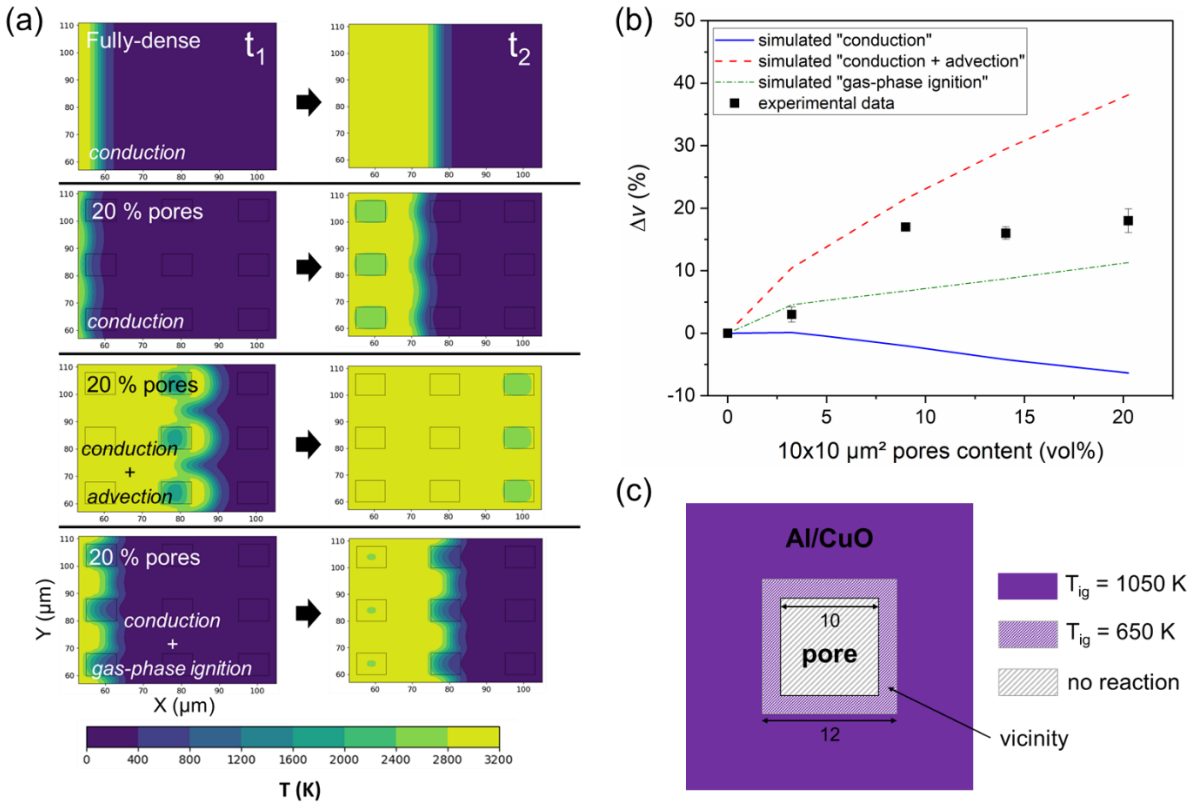

Figure 6. *(a) 2D maps of the temperature taken at two different times (t_1 and t_2) of the simulation, for fully dense and porous nanolaminates with 20% volume fraction, considering pure conduction, (conduction + advection) in pores, or gas-phase ignition at the vicinity of pores. (b) Simulated propagation speed enhancement with 20 % pores content with different configurations: pure conduction (solid blue line), (conduction + advection) in pores (dashed red line) and (conduction + "gas-phase ignition") (dashed green line). Black squares represent the experimental data. (c) Illustration of "gas-phase ignition" configuration, showing the spatial distribution of the ignition temperature T_{ig} in the "vicinity" of the pores.*

4. Conclusion

Incorporating micron sized pores in fully dense Al/CuO nanolaminates results in a faster burn rate (burn rate enhancement of 18% for pores loading of 20 vol%) while the flame temperature remains the same. Interestingly and unexpectedly, microscopic observations of the burning front in porous nanolaminate show hot-spots around each pore in the upstream of the

flame but no advection could be observed; as first conclusion conduction remains the dominant heat transfer mechanism in dense thermite configuration (80 % TMD). The cause of burn rate enhancement when pores are embedded into the nanolaminate can be explained by two possible effects: 1) the establishment of convection of the trapped air inside the pores thus improving the heat and mass transfer to unreacted material. This effect is also supported by the fact that increasing the pore size, the air does not heat up much and burn rate does not increase much; 2) a modification of the reaction chemistry around each micron sized pores leading to a lowering of the ignition threshold. The air inside the pores also acts as oxidizer as it can diffuse and react readily upon adsorbing to exposed Al or Al_2O_3. This gas phase mediated reaction mechanism occurs at lower temperature than the diffusion-based mechanism of the aluminum cations and oxide anions across the alumina shell as in fully dense Al/CuO nanolaminates. The critical size of the pores beyond which their beneficial effect disappears is difficult to estimate, but, this study showed that 100 × 100 μm² pores has no effect on the combustion with an average burn rate increase of only ~4% compare to fully dense nanolaminate part.

ASSOCIATED CONTENT

The Supporting Information is available free of charge on the ACS Publications website at DOI:

Optical image of a typical Al/CuO laminate with air-filled pores (Figure S1); corrected configurations of laminates with different porosities (Table S1); Thermo-physical properties used in the model for Al/CuO laminates and air-filled pores (Table S2); Condition parameters used in the model to simulate the reaction (Table S3).

Author contributions

T.W. prepared all samples and performed all characterization measurements. T.W. and C.R drafted the manuscript. B.J. performed and drafted the flame propagation model and assisted T.W. in EDX analysis. H.W. performed high speed in operando microscopy/thermometry. S.P. assisted T.W. in thermite deposition. M.Z and A.E. provided support for the manuscript preparation. C.R. supervised this research.

Funding Sources

C.R. received funding from the European Research Council (ERC) under the European Union's Horizon 2020 research and innovation program (grand agreement No. 832889 - PyroSafe). University of California authors were supported by the AFOSR.

Competing financial interests

The authors declare no competing financial interests.

Acknowledgements

The authors grateful acknowledge support from the European Research Council (H2020 Excellent Science) Researcher Award (grant 832889 – PyroSafe). This work was also supported by LAAS-CNRS technology platform, a member of Renatech network. University of California authors were supported by the AFOSR. The authors also acknowledge the help from Claudie Josse in SEM and EDX analysis.

References

1. Yetter, R. A.; Risha, G. A.; Son, S. F., Metal particle combustion and nanotechnology. *P Combust Inst* **2009,** *32*, 1819-1838.
2. Rossi, C., *Al-based Energetic Nanomaterials : design, manufacturing, properties and applications*. Wiey: London, 2015; Vol. 2.
3. Koch, E. C.; Knapp, S., Thermites - Versatile Materials. *Propell Explos Pyrot* **2019,** *44* (1), 7-7.
4. Umbrajkar, S. M.; Schoenitz, M.; Dreizin, E. L., Exothermic reactions in Al-CuO nanocomposites. *Thermochim Acta* **2006,** *451* (1-2), 34-43.
5. Rossi, C., Engineering of Al/CuO Reactive Multilayer Thin Films for Tunable Initiation and Actuation. *Propellants, Explosives, Pyrotechnics* **2019,** *44* (1), 94-108.
6. Egan, G. C.; Mily, E. J.; Maria, J. P.; Zachariah, M. R., Probing the Reaction Dynamics of Thermite Nanolaminates. *J Phys Chem C* **2015,** *119* (35), 20401-20408.
7. Lahiner, G.; Nicollet, A.; Zapata, J.; Marín, L.; Richard, N.; Djafari-Rouhani, M.; Rossi, C.; Estève, A., A diffusion–reaction scheme for modeling ignition and self-propagating reactions in Al/CuO multilayered thin films *J Appl Phys* **2017,** *122* (15).
8. Zhang, Y. Q.; Sui, H. T.; Li, Y. N.; Wen, J. Z., Energetic characteristics of the Al/CuO core-shell composite micro-particles fabricated as spherical colloids. *Thermochim Acta* **2020,** *689*.
9. Prakash, A.; McCormick, A. V.; Zachariah, M. R., Tuning the reactivity of energetic nanoparticles by creation of a core-shell nanostructure. *Nano Lett* **2005,** *5* (7), 1357-1360.
10. Palussiere, S.; Cure, J.; Nicollet, A.; Fau, P.; Fajerwerg, K.; Kahn, M. L.; Esteve, A.; Rossi, C., The role of alkylamine in the stabilization of CuO nanoparticles as a determinant of the Al/CuO redox reaction. *Phys Chem Chem Phys* **2019,** *21* (29), 16180-16189.

11. Calais, T.; Bancaud, A.; Estève, A.; Rossi, C., Correlation between DNA Self-Assembly Kinetics, Microstructure, and Thermal Properties of Tunable Highly Energetic Al-CuO Nanocomposites for Micro-Pyrotechnic Applications. *ACS Appl. Nano Mater.* **2018,** *1* (9), 4716-4725.
12. Chen, Y. J.; Ren, W.; Zheng, Z. L.; Wu, G. G.; Hu, B.; Chen, J. H.; Wang, J. X.; Yu, C. P.; Ma, K. F.; Zhou, X. L.; Zhang, W. C., Reactivity adjustment from the contact extent between CuO and Al phases in nanothermites. *Chem Eng J* **2020,** *402*, 9.
13. Sui, H. T.; Huda, N.; Shen, Z. K.; Wen, J. Z., Al-NiO energetic composites as heat source for joining silicon wafer. *J Mater Process Tech* **2020,** *279*.
14. Wu, T.; Wang, X. Z.; Zavalij, P. Y.; DeLisio, J. B.; Wang, H. Y.; Zachariah, M. R., Performance of iodine oxides/iodic acids as oxidizers in thermite systems. *Combust Flame* **2018,** *191*, 335-342.
15. Wang, S.; Schoenitz, M.; Grinshpun, S. A.; Yermakov, M.; Dreizin, E. L., Biocidal effectiveness of combustion products of iodine-bearing reactive materials against aerosolized bacterial spores. *J Aerosol Sci* **2018,** *116*, 106-115.
16. Glavier, L.; Nicollet, A.; Jouot, F.; Martin, B.; Barberon, J.; Renaud, L.; Rossi, C., Nanothermite/RDX-Based Miniature Device for Impact Ignition of High Explosives. *Propell Explos Pyrot* **2017,** *42* (3), 307-316.
17. Fu, S.; Shen, R. Q.; Zhu, P.; Ye, Y. H., Metal-interlayer-metal structured initiator containing Al/CuO reactive multilayer films that exhibits improved ignition properties. *Sensor Actuat a-Phys* **2019,** *292*, 198-204.
18. Ardila Rodríguez, G. A.; Suhard, S.; Rossi, C.; Estève, D.; Fau, P.; Sabo-Etienne, S.; Mingotaud, A. F.; Mauzac, M.; Chaudret, B., A microactuator based on the decomposition of an energetic material for disposable lab-on-chip applications: fabrication and test. *J Micromech Microeng* **2008,** *19* (1), 015006.
19. Nicollet, A.; Salvagnac, L.; Baijot, V.; Estève, A.; Rossi, C., Fast circuit breaker based on integration of Al/CuO nanothermites. *Sensors and Actuators A: Physical* **2018,** *273*, 249-255.
20. Apperson, S. J.; Bezmelnitsyn, A. V.; Thiruvengadathan, R.; Gangopadhyay, K.; Gangopadhyay, S.; Balas, W. A.; Anderson, P. E.; Nicolich, S. M., Characterization of Nanothermite Material for Solid-Fuel Microthruster Applications. *J Propul Power* **2009,** *25* (5), 1086-1091.
21. Zhu, P.; Hou, G.; Wang, H. Y.; Xu, C.; Zhao, S. F.; Shen, R. Q., Design, Preparation, and Performance of a Planar Ignitor Inserted With PyroMEMS Safe and Arm Device. *J Microelectromech S* **2018,** *27* (6), 1186-1192.
22. Staley, C. S.; Raymond, K. E.; Thiruvengadathan, R.; Apperson, S. J.; Gangopadhyay, K.; Swaszek, S. M.; Taylor, R. J.; Gangopadhyay, S., Fast-Impulse Nanothermite Solid-Propellant Miniaturized Thrusters (vol 29, pg 1400, 2013). *J Propul Power* **2015,** *31* (1), 483-483.
23. Puchades, I.; Hobosyan, M.; Fuller, L. F.; Liu, F.; Thakur, S.; Martirosyan, K. S.; Lyshevski, S. E., MEMS microthrusters with nanoenergetic solid propellants. *In 14th IEEE International Conference on Nanotechnology* **2014**.
24. Sullivan, K. T.; Bastea, S.; Kuntz, J. D.; Gash, A. E., A pressure-driven flow analysis of gas trapping behavior in nanocomposite thermite films. *J Appl Phys* **2013,** *114* (16).
25. Sullivan, K. T.; Zhu, C.; Duoss, E. B.; Gash, A. E.; Kolesky, D. B.; Kuntz, J. D.; Lewis, J. A.; Spadaccini, C. M., Controlling Material Reactivity Using Architecture. *Adv Mater* **2016,** *28* (10), 1934-+.
26. Pantoya, M. L.; Levitas, V. I.; Granier, J. J.; Henderson, J. B., Effect of Bulk Density on Reaction Propagation in Nanothermites and Micron Thermites. *J Propul Power* **2009,** *25* (2), 465-470.
27. Ahn, J. Y.; Kim, J. H.; Kim, J. M.; Lee, D. W.; Park, J. K.; Lee, D.; Kim, S. H., Combustion characteristics of high-energy Al/CuO composite powders: The role of oxidizer structure and pellet density. *Powder Technol* **2013,** *241*, 67-73.
28. Sanders, V. E.; Asay, B. W.; Foley, T. J.; Tappan, B. C.; Pacheco, A. N.; Son, S. F., Reaction propagation of four nanoscale energetic composites (Al/MoO3, Al/WO3, Al/CuO, and Bi2O3). *J Propul Power* **2007,** *23* (4), 707-714.
29. Bockmon, B. S.; Pantoya, M. L.; Son, S. F.; Asay, B. W.; Mang, J. T., Combustion velocities and propagation mechanisms of metastable interstitial composites. *J Appl Phys* **2005,** *98* (6).

30. Zapata, J.; Nicollet, A.; Julien, B.; Lahiner, G.; Esteve, A.; Rossi, C., Self-propagating combustion of sputter-deposited Al/CuO nanolaminates. *Combust Flame* **2019,** *205*, 389-396.
31. Mursalat, M.; Huang, C.; Julien, B.; Schoenitz, M.; Esteve, A.; Rossi, C.; Dreizin, E. L., Low-Temperature Exothermic Reactions in Al/CuO Nanothermites Producing Copper Nanodots and Accelerating Combustion. *Acs Appl Nano Mater* **2021,** *4* (4), 3811-3820.
32. Wang, H. Y.; Kline, D. J.; Zachariah, M. R., In-operando high-speed microscopy and thermometry of reaction propagation and sintering in a nanocomposite. *Nat Commun* **2019,** *10*.
33. Wang, H. Y.; Rehwoldt, M.; Kline, D. J.; Wu, T.; Wang, P.; Zachariah, M. R., Comparison study of the ignition and combustion characteristics of directly-written Al/PVDF, Al/Viton and Al/THV composites. *Combust Flame* **2019,** *201*, 181-186.
34. Wang, H. Y.; Julien, B.; Kline, D. J.; Alibay, Z.; Rehwoldt, M. C.; Rossi, C.; Zachariah, M. R., Probing the Reaction Zone of Nanolaminates at similar to mu s Time and similar to mu m Spatial Resolution. *J Phys Chem C* **2020,** *124* (25), 13679-13687.
35. Lanthony, C.; Guiltat, M.; Ducere, J. M.; Verdier, A.; Hemeryck, A.; Djafari-Rouhani, M.; Rossi, C.; Chabal, Y. J.; Esteve, A., Elementary Surface Chemistry during CuO/Al Nanolaminate-Thermite Synthesis: Copper and Oxygen Deposition on Aluminum (111) Surfaces. *Acs Appl Mater Inter* **2014,** *6* (17), 15086-15097.
36. Abdallah, I.; Zapata, J.; Lahiner, G.; Warot-Fonrose, B.; Cure, J.; Chabal, Y.; Esteve, A.; Rossi, C., Structure and Chemical Characterization at the Atomic Level of Reactions in Al/CuO Multilayers. *ACS Applied Energy Materials* **2018,** *1* (4), 17-62.
37. DeLisio, J. B.; Yi, F.; LaVan, D. A.; Zachariah, M. R., High Heating Rate Reaction Dynamics of Al/CuO Nanolaminates by Nanocalorimetry-Coupled Time-of-Flight Mass Spectrometry. *J Phys Chem C* **2017,** *121* (5), 2771-2777.
38. Wang, H. Y.; Kline, D. J.; Rehwoldt, M. C.; Zachariah, M. R., Carbon Fibers Enhance the Propagation of High Loading Nanothermites: In Situ Observation of Microscopic Combustion. *Acs Appl Mater Inter* **2021,** *13* (26), 30504-30511.
39. Tichtchenko, E.; Estève, A.; Rossi, C., Modeling the self-propagation reaction in heterogeneous and dense media: Application to Al/CuO thermite. *Combust Flame* **2021,** *228*, 173-183.
40. Jian, G. Q.; Chowdhury, S.; Sullivan, K.; Zachariah, M. R., Nanothermite reactions: Is gas phase oxygen generation from the oxygen carrier an essential prerequisite to ignition? *Combust Flame* **2013,** *160* (2), 432-437.